COMMUNICATION

Microfluidic Manipulation of Core/Shell Nanoparticles for Oral Delivery of Chemotherapeutics: A New Treatment Approach for Colorectal Cancer

Mohammad Mahdi Hasani-Sadrabadi, Shahrouz Taranejoo, Erfan Dashtimoghadam, Ghasem Bahlakeh, Fatemeh Sadat Majedi, Jules John VanDersarl, Mohsen Janmaleki, Fatemeh Sharifi, Arnaud Bertsch, Kerry Hourigan, Lobat Tayebi, Philippe Renaud,* and Karl I. Jacob**

Colon cancer is one of the most prevalent cancers today that is affecting people at an increasing rate. Currently, the lifetime risk of developing colon cancer runs at 5%–6%.[1] Considering the growing rate of colorectal cancer, considerable scientific effort has been applied to find effective therapeutic approaches.[2] The conventional chemotherapy affects nontumor cells and adverse effects to normal tissues/organs are unavoidable. Due to these side effects, survival rate from cytotoxic chemotherapy is further limited. Nanoparticulate drug delivery systems make the chemotherapeutic approaches more selective with less off-target toxicity. A central challenge in nanomedicine is the fine design of nanoparticles for their desired physicochemical properties in a reproducible manner. Thus, a significant part of this research has been focused on developing smart targeting drug delivery systems, to both minimize side effects and increase drug efficacy.[3] Oral drug delivery is an important administration pathway as it improves patient compliance and is self-administrable, which allows for more regular dosing schedules at a lower cost. Oral chemotherapeutics can also lead to lower toxicity and improved efficacy.[4] Due to the pH variations in the gastrointestinal tract during oral drug administration,[5] employing pH-sensitive polymers as carriers can result in more specific chemotherapeutic delivery for cancer therapy.[5–8] Polymers and copolymers such as methacrylic acid and methylacrylate or ethylacrylate are typical pH responsive polymeric materials employed in the preparation of extended release oral administered drugs for cancer therapy.[7,9,10] These copolymers are insoluble at low pH but dissolve at high pH, triggering the encapsulated drugs or inner core to be released.[10] Despite recent advances in chemotherapeutic delivery systems for colon cancer, most researches have focused on conventional bulk mixing, which results in polydisperse nanoparticles (NPs).[8,11,12] However, attaining more precise drug release profiles requires a reproducible approach to fabricate finely tuned nanocarriers with a narrow size distribution and

Dr. M. M. Hasani-Sadrabadi, K. I. Jacob
Parker H. Petit Institute for Bioengineering and Bioscience
G. W. Woodruff School of Mechanical Engineering
and School of Materials Science and Engineering
Georgia Institute of Technology
Atlanta, GA 30332-0295, USA
E-mail: karl.jacob@mse.gatech.edu

S. Taranejoo, K. Hourigan
Department of Chemical Engineering
Monash University
Melbourne, VIC 3168, Australia

S. Taranejoo, K. Hourigan
Laboratory for Biomedical Engineering/Fluids
Laboratory for Aeronautical and Industrial Research
Department of Mechanical and Aerospace Engineering
Faculty of Engineering
Monash University
Melbourne, VIC 3168, Australia

Dr. E. Dashtimoghadam, L. Tayebi
Department of Developmental Sciences
Marquette University School of Dentistry
Milwaukee, WI 53201, USA
E-mail: lobat.tayebi@marquette.edu

Prof. G. Bahlakeh
Department of Chemical Engineering
Amirkabir University of Technology
Tehran 49417-15344, Iran

F. S. Majedi
Department of Bioengineering
University of California at Los Angeles
Los Angeles, CA 90095, USA

Dr. J. J. VanDersarl, A. Bertsch, P. Renaud
Laboratoire de Microsystemes (LMIS4)
Institute of Microengineering and Institute of Bioengineering
École Polytechnique Fédérale de Lausanne (EPFL)
CH-1015 Lausanne, Switzerland
E-mail: philippe.renaud@epfl.ch

M. Janmaleki
Medical Nanotechnology and Tissue Engineering Research Center
Shahid Beheshti University of Medical Sciences
Tehran 19857-17444, Iran

F. Sharifi
Department of Mechanical Engineering
Sharif University of Technology
Tehran 11365-11155, Iran

Prof. L. Tayebi
Biomaterials and Advanced Drug Delivery Laboratory
Stanford University School of Medicine
Palo Alto, CA 94304, USA

DOI: 10.1002/adma.201502697

predetermined properties. We have recently introduced a microfluidic technique to synthesize monodisperse chitosan-based NPs for cancer therapy applications.[8,12] Compared to bulk mixing process, microfluidic systems can synthesize the nanoparticles in a well-controlled, reproducible, and high-throughput manner. Moreover, microfluidic systems, by mixing dissimilar materials (with distinct functional groups) at varying ratios, provide better process control and a much better solution for the challenge in finding the correct formulation for delivering therapeutic agents to specific sites in the body.

Chitosan derivatives are widely used in drug delivery applications due to their outstanding biological characteristics.[13] Here we employ a hydrophobically modified chitosan (HMCS) derivative, *N*-palmitoyl chitosan, to improve the loading of hydrophobic anticancer drugs.[14] Moreover, *N*-palmitoyl chitosan chains allow for NPs to be shaped via self-assembly, avoiding problems related to the removal of chemical cross-linking agents.[8,15,16] Microfluidic platforms, benefiting from a controlled mixing regime, provide adjustable drug encapsulation efficiency and release rate from self-assembled HMCS.[8,12,17] In this study, we used microfluidic techniques to design well-controlled monodisperse HMCS NPs coated by a pH-responsive layer (Eudragit FS 30D) with an adjustable thickness. The NPs' behavior was assessed as they were exposed to variant pH conditions that closely simulate the digestive tract environment. Quantum mechanics (QM) and classical molecular dynamics (MD) simulations were also performed to investigate the molecular interactions governing the behavior of the chitosan–Eudragit layered system.

Details of the materials and methods used in this work are provided in the Supporting Information. Schematic representations of the microfluidic platforms are shown in **Figure 1**a. The nanoparticle cores are created in the first microreactor, where hydrodynamically focused flow precisely controls the mixing time of the two solutions (HMCS and water), resulting in monodispersed nanoparticles with precisely controlled properties. These particles are then coated in a Tesla micromixer, where they are sealed with a Eudragit (pH-sensitive poly(methyl methacrylate) (PMMA) derivative) shell. The micromixer inputs (flow ratios) determine the reactor conditions, and thus the nanocapsule properties. The design of the Tesla micromixer was finalized using COMSOL Multiphysics software to investigate the flow/concentration profiles. Using 2D modeling of 10 individual mixer units, the continuity and constitutive Navier–Stokes equations along with convection–diffusion equation were solved using the finite element method for various geometries. The inlet boundary condition is approximated by the sheath flow and core flow concentrations, and flow rates. Tesla mixers use the Coanda effect to bend fluid stream lines and increase the mixing effects. As flow enters the micromixer, part of it deflects toward the side narrow channel due to the Coanda effect, while the remaining fluid flows through the curved-section until these two sub-flows merge. This recombined flow then experiences the Coanda effect again, and this separation and mixing continues until the flow reaches the outlet. The concentration distribution for this Tesla micromixer is shown in Figure 1b-i. For this flow condition, full mixing is obtained after passing two cell-pairs. The velocity stream lines are shown in Figure 1b-iii.

Increasing the flow ratio (volumetric ratio of sheath flow to main flow from 0.03 to 0.3) in the microreactors caused a strong increase in total NP diameter for both neat and PTX-loaded particles (Figure 1c-i,c-iv). Figure 1c-ii shows the shell thickness for the coated NPs increasing with increasing flow ratio. For instance, by increasing the flow ratio in the Tesla micromixer (μR2) from 0.07 to 0.3 while keeping the flow ratio constant for the first micromixer (0.03), the average shell thickness increased from 8 to more than 22 nm. A more complex trend in zeta potential variation was observed. As shown in Figure 1c-iii, the highest zeta potential value (+10 mV) occurred for the NPs synthesized at the lowest flow ratio in reactor 2 (0.07). This is consistent with the shell thickness results. The Eudragit supportive layer and HMCS core have negative and positive charges, respectively. Hence, decreasing the shell thickness, as a direct consequence of decreasing the flow ratio in micromixer 2, resulted in NPs with a higher net positive charge, and an increased zeta potential.

Employing the microfluidic process is a significant improvement over the traditional bulk mixing procedures, and results in NPs with smaller diameter for both uncoated and masked NPs at all flow ratios. A broad distribution of residence times in the turbulent regime and variations of local pH at bulk mixing condition are considered the main reasons for such nonuniformity in bulk NPs.[12,15] The first microreactor establishes a well-controlled hydrodynamically focused mixing region with short and narrowly distributed residence times, defined by the input flow rates and ratios, which generates smaller NPs with uniform diameter and microstructure.[8,12,15] In the first micromixer (cross-junction), the pH increases through diffusion of the basic water into the aqueous polymer stream, which leads to HMCS amine group deprotonation and aggregation of the macromolecules. A narrow distribution of residence times provided by on-chip diffusion mixing gives the opportunity for the polymer chains to benefit from similar reaction times.[8] Solution pH controls the balance between electrostatic repulsion and hydrophobic attraction forces, so the time scale associated with the pH rearrangement determines the self-assembly time scale, which is short in the microfluidic device and thus generates small and uniform NPs (Figure 1d-i).[8]

In microreactor 2, mixing and laminar flow are the predominant routes of mass transfer, where reactions mainly occur in the microscale rather than the molecular scale. This resulted in more nonuniformity in shell thickness and morphology of the masked NPs. The very slow kinetic diffusion of Eudragit chains prevents the cross-junction "t" microreactor design used to create the NP cores from being used to coat the NPs.[18] This limitation leads to the design of the Tesla mircoreactor with alteration in shape, residence time, and thus the predominant route of mass transfer. Still, the NPs coated with Eudragit in the microreactor were more uniformly coated than those coated via bulk mixing.

In order to better understand the molecular interactions in the Eudragit–chitosan core–shell NPs, MD simulations were conducted on a 3D cell consisting of Eudragit and chitosan chains by use of COMPASS (condensed-phase optimized molecular potentials for atomistic simulation studies) force field. Equilibration of the simulated structures was first checked by monitoring time evolution of the potential energy as well as temperature of the cell (see Figure SI-3 of the Supporting Information). As shown, the total potential energy and temperature fluctuate slightly around an average value,

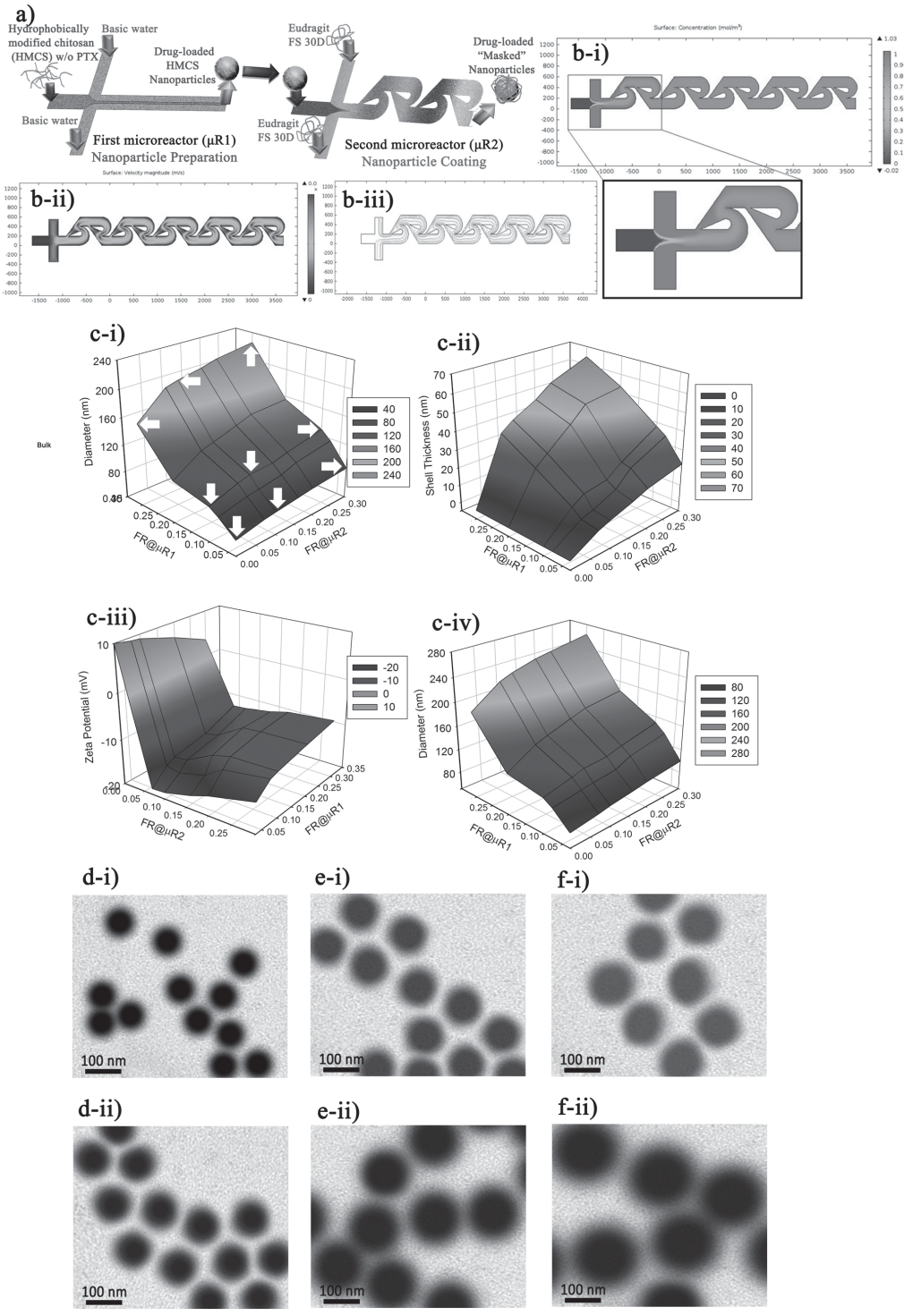

Figure 1. a) A schematic representation of the dual microfluidic platform used to synthesis tunable core–shell nanoparticles: a cross-junction microfluidic device used to control formation of chitosan-based NPs from polymer core flow, which hydrodynamically focused with sheath flows of water at basic pH (μR1), and a Tesla micromixer to make Eudragit FS 30D coated onto NPs (μR2). b) COMSOL simulation results on b-i) concentration distributions, b-ii) velocity distributions, and b-iii) velocity streamlines for the Tesla micromixer. c) 3D plots of NPs' experimental characteristics, which were adjusted via the parameters of μR1 and μR2: c-i) NPs' diameter without PTX, c-ii) shell thickness, c-iii) zeta potential, c-iv) diameter with PTX. The white arrows represent the positions of NP samples selected for further experiments. d–e) Transmission electron microscopy images of i) uncoated and ii) masked HMCS NPs; d-i) μR1:0.03, no coating, d-ii) μR1:0.03 and μR2: 0.10, e-i) μR1:0.10, no coating, e-ii) μR1:0.10, μR2: 0.10, f-i) R1: bulk, no coating, f-ii) R1: bulk, μR2: 0.10.

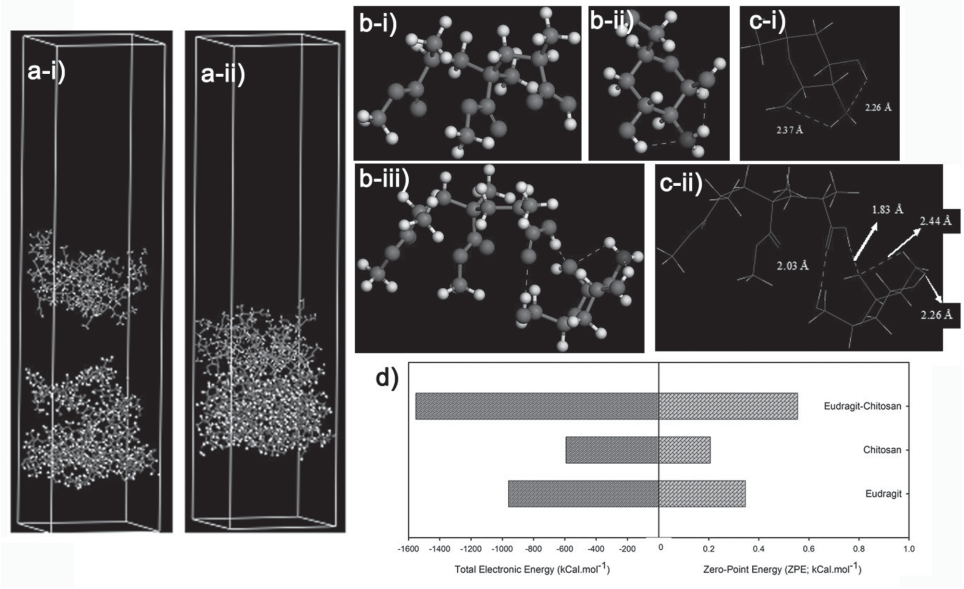

Figure 2. a) Eudragit–chitosan layered structure a-i) initial structure and a-ii) after 600 ps *NVT* MD simulations. Polymer chains are shown inside the simulation cell with periodic boundary conditions. All atoms of Eudragit and chitosan polymers are in line, and ball and stick style, respectively. b) B3LYP/6-311G** optimized model structure of b-i) Eudragit, b-ii) chitosan, and b-iii) Eudragit–chitosan cluster. Hydrogen bonding interactions are shown as dashed lines; all atoms are in ball and stick model. c) Hydrogen bond length in B3LYP/6-311G** optimized model structure of c-i) chitosan, and (c-ii) Eudragit–chitosan cluster. Hydrogen bonding interactions are shown as dashed lines. All atoms are in line style. The color code for all items: carbon in gray, oxygen in red, nitrogen in blue, and hydrogen in white. d) Total electronic energy (Hartrees) and ZPE (Hartrees) (kcal mol^{-1}) for B3LYP/6-311G** optimized Eudragit, chitosan, and Eudragit–chitosan cluster structures.

which indicates an equilibrium condition has been achieved. The final structure from the last 100 ps *NVT* (moles (*N*), volume (*V*), and temperature (*T*) are conserved for the canonical ensemble) MD simulation of layered Eudragit–chitosan cell is shown in **Figure 2**a. To make a better comparison, the initial layered structures used for MD simulation are also shown. It is obvious that in comparison with the initial 3D cell, the distance between Eudragit and chitosan layers in the equilibrated cell became closer. Such an observation is attributed to the strong affinity of Eudragit and chitosan chains, as confirmed quantitatively by the binding energy, and the strong intermolecular hydrogen bonding interactions between Eudragit and chitosan. Figure 2a shows both the initial and final structures with periodic boundary conditions, which clearly demonstrate the tendency of Eudragit and chitosan chains to interface tightly.

First principle QM simulations were applied for the three molecular systems including Eudragit, chitosan, and Eudragit–chitosan clusters. QM simulations were specifically utilized to assess the intermolecular interaction energy between Eudragit and chitosan, which allows us to determine their affinity for each other. Figure 2b shows the final energy-minimized model structures for Eudragit, chitosan, as well as Eudragit–chitosan, resulted from B3LYP/6-311G** level of theory. We find that the optimized monomer structure of Eudragit is not able to form any intramolecular hydrogen bonds, while chitosan can form intramolecular hydrogen bonds between amine ($-NH_2$) and hydroxyl (—OH) groups. In the simulation, hydrogen bonds are assumed when two hydrogen donor and hydrogen acceptor atoms satisfy the following geometrical conditions: (1) the distance between a hydrogen donor atom and hydrogen acceptor atom is less than 2.5 Å, and (2) the hydrogen donor–hydrogen–hydrogen acceptor angle is greater than 90°. For the single chitosan structure, the nitrogen atom in the amine groups acts as both hydrogen donor and hydrogen acceptor, while the oxygen atom in one of hydroxyl groups directly attached to the chitosan backbone acts as a hydrogen donor in hydrogen bond formation, and the oxygen atoms in the other hydroxyl group directly bonded to the polymer backbone appear as hydrogen acceptor atoms.

In the case of Eudragit–chitosan cluster model, two intermolecular hydrogen bonding interactions are formed between Eudragit and chitosan units, in which oxygen atoms in the Eudragit carboxylic group act as hydrogen bond donor and acceptor atoms, and hydroxyl group attached to the backbone via methyl group and hydroxyl group directly attached to the backbone act as hydrogen donor and acceptor atoms, respectively. These types of interactions show that Eudragit polymers are able to interact via their methacrylic acid groups with chitosan. The intramolecular hydrogen bonds formed in chitosan-only structures and in Eudragit–chitosan clusters are the same.

In order to gain further insights into the interaction between Eudragit and chitosan, length of the hydrogen bonding interactions was examined (Figure 2c). The hydrogen bond lengths obtained clearly indicate that intramolecular hydrogen bond length in chitosan and also intermolecular hydrogen bonds in chitosan interacting with Eudragit are almost the same, which signifies that interaction of chitosan with Eudragit does not significantly influence the strength of intramolecular hydrogen bonding interactions within chitosan. However, as the intermolecular hydrogen bond length in Figure 2c-ii shows, the length of the Eudragit–chitosan hydrogen bonds is shorter than that of intramolecular hydrogen bonds within chitosan, which

demonstrates the stronger binding affinity between Eudragit and chitosan chains. The findings of the QM and MD simulation results are consistent with each other.

Total electronic energy and zero-point energy (ZPE) corrected total electronic energy of the final B3LYP/6-311G** optimized Eudragit, chitosan, and Eudragit–chitosan structures are shown in Figure 2d. From these total energy levels, the interaction energy (ΔE) values for the Eudragit–chitosan cluster model were calculated to be –11.23 kcal mol^{-1} ($\Delta E_{\text{electronic}}$) and –9.60 kcal mol^{-1} (ΔE_{ZPE}). We observed that the interaction energies are negative, which is indicative of the fact that Eudragit and chitosan chains tend to be located in the vicinity of each other and interact together. The Eudragit–chitosan affinity is associated with their intermolecular interactions, especially the hydrogen bonding displayed in Figure 2b.

Figure SI-4 (Supporting Information) shows the hydrodynamic diameter of synthesized core–shell NPs over time under various pH conditions. The pH alterations were intended to somewhat mimic the digestive tract. In the gastrointestinal tract, the intraluminal pH increases from highly acidic medium (pH 1–2 which increases to 4 during digestion) in the stomach to about pH 7.4 in the terminal ileum of the small intestine. This change is followed by a pH drop to 5.7 in the caecum (colon).[19] It is worth noting that no significant differences were found in the gastrointestinal pH levels between normal subjects and people suffering from colorectal carcinoma.[20]

Generally, the size of NPs depends on the number of polymer chains as well as their swelling states. It has been shown that the swelling state is highly affected by the compactness of self-assembled NPs, which can be controlled by changing the flow ratio on microfluidic platforms.[15] The probability of hydrophobic side chains competing with intramolecular interactions is highly influenced by the mixing time, where it has been shown that longer mixing time results in less compact NPs.[15] As shown in Figure SI-4 (Supporting Information), NPs synthesized at lower flow ratios in μR1 (t-shaped microreactor) show higher stability, which is due to their more compact structure. In comparison with microfluidic NPs, less compact bulk-synthesized NPs show less resistance to chemical and physiological alterations, leading to more swelling when exposed to pH alteration. Increasing the pH to 7.4 is associated with an initial NP swelling, and is followed by a significant decrease in the size of the NPs. Early stage increase in diameter of the NPs can be interpreted as the swelling of the Eudragit layer in the solubilizing pH medium. Subsequently, gradual dissolution of the Eudragit layer in the neutral medium leads to a drop in the size of the NPs. It should be noticed that the observed differences in the size of the NPs are related to their different compactness. After the removal of the Eudragit layer, the next change in pH from 7.4 to 5.5 results in a significant increase in the size of NPs. Swelling of the NPs in this stage is due to the electrostatic repulsion of the highly protonated HCMS chains, which ends in dissolution of the swollen NPs (Figure SI-4, Supporting Information). Bulk-synthesized NPs coated at a flow ratio (FR) of 0.1 were found to show the most significant and rapid size alterations. The overall diameter changes of the NPs were less significant over the first pH transition (pH 4–7.4) compared to the second transition (pH 7.4–5.5). This effect was more pronounced for the microfluidic NPs, which disclose the ability of the microfluidic synthesis method to produce dense and compact NPs.[15] Over the second pH transition, the removal of the shell layer causes their size to change significantly.

The dynamic size of microfluidic core–shell nanoparticles formed at μR1:0.03 and μR2:0.10 in the simulated gastric and intestinal fluids was also investigated and shown in Figure SI-5 (Supporting Information). In addition, the stability of core–shell nanoparticles (μR1:0.03 and μR2:0.10) after incubation for 120 h in the gastric simulated (pH = 4) and intestinal simulated (pH = 7.4) conditions is examined (Figure SI-6, Supporting Information). Figure SI-7 (Supporting Information) compares the drug release profiles from microfluidic-coated NPs with NPs coated in the bulk process and uncoated NPs. The results clearly show that microfluidic-coated NPs are significantly more effective compared to other NPs in releasing the therapeutic agent in the required low pH region for colorectal cancer after experiencing a pH history of low and high pH domains.

We also show the applicability of this approach for other charged polymers. As shown in Figure SI-8 (Supporting Information), we coated chitosan-based bulk-synthesized and microfluidic-synthesized NPs by Alginate (as a representative charged natural polymer) in addition to Eudragit (as a representative charged synthetic polymer). We also made polyethylenimine(PEI)/DNA nanoplexes and coated them with Alginate and Eudragit using the same microfluidic platform. The results obtained with other combinations are similar to those of Eudragit coated chitosan NPs, but show that NPs of other core and shell material combinations can be considered for other similar drug delivery applications.

Figure 3a shows the in vitro release profiles of different PTX-loaded NPs over the sequential changes in pH (4, 7.4, and 5.5) at 37 °C. The relatively rapid initial drug release from uncoated NPs (both microfluidic-synthesized and bulk-synthesized particles), more than 30% in the first 24 h, has been typically reported for PTX-loaded chitosan-based NPs at low pH medium.[21,22] In the self-assembled NPs, drug molecules may have been partially loaded in the outer layers of particles, specifically, in the case of bulk-synthesized NPs, resulting in their accelerated release. Core–shell NPs, which were prepared on the dual microfluidic platforms, have highly useful drug release profiles for colorectal treatment, limited burst release at low pH, followed by more sustained release profiles at the next successive pH levels (7.4 and 5.5).

As previously stated, using microfluidics provides the possibility to synthesize more compact and smaller NPs in comparison with bulk-synthesized particles. Hence, the slower release rate of the microfluidic prepared NPs is due to their relatively more compact microstructures.[15] Coating the NPs with Eudragit, as shown in Figure 3a, strongly affected the release profile. The pH-sensitive Eudragit outer layer, which is insoluble in low pH environment, hinders PTX diffusion to the surface of the NPs in early stage of release and reduces burst release in the acidic medium. In the case of uncoated NPs, the major part of the encapsulated PTX is released in the first stage (acidic pH), an effect which is more pronounced for the bulk-synthesized NPs. Obviously, the release rate of the microfluidic NPs accelerated after increasing pH from 4 to 7.4, which is in contrast to the decreased release rate of the uncoated NPs after a similar pH transition. This trend is attributed to the dissolution and higher swelling ratio of Eudragit layer

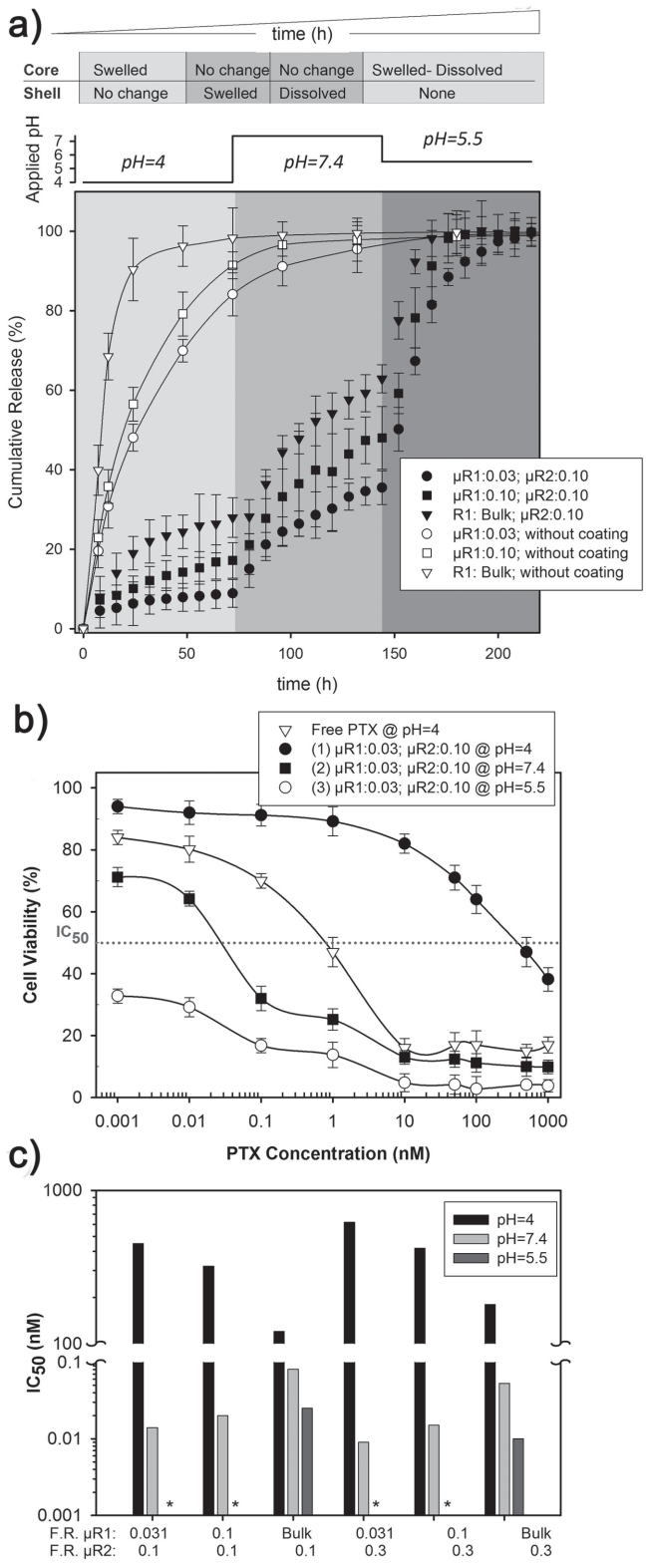

Figure 3. a) Cumulative in vitro release of PTX from uncoated (empty symbols) as well as coated (filled symbols) chitosan-based NPs after sequential change in pH (4, 7.4, and 5.5) at 37 °C (mean ± SD, $n = 3$ independent experiments). b) Cell viability of Caco-2 cells after 72 h exposure to free PTX as well as PTX-loaded NPs as a function of pH at 37 °C. c) IC_{50} values for different types of uncoated/coated NPs after sequential incubation at different pH. Lower IC_{50} value indicate more potent therapeutic agent. * indicates $IC_{50} < 0.001$. Results presented as mean value ± SD, $n = 3$ independent experiments.

at neutral pH in comparison with acidic pH. Such pH-responsive release behavior has been reported by other researchers.[23,24]

Thus, coating the NPs with pH-sensitive layer gives them the ability to bypass the acidity of gastric fluid without releasing considerable amounts of the loaded drug.[24] After dissolution of the supportive layer at higher pH, modified chitosan core forms a gel like insoluble structure; hence, the rate of drug release is controlled.[25] Interestingly, a further acceleration of release rate was observed for the microfluidic NPs after decreasing pH from 7.4 to 5.5. Over the last release stage, protonation of amino groups on chitosan chains causes swelling of NPs, which ultimately results in an increased rate of PTX release.[26]

The effect of unloaded NPs at different concentrations (50–800 μg mL^{-1}) on the viability of two kinds of cells (Caco-2 and mouse embryonic fibroblasts (MEF)) after 72 h using the (3-(4,5-dimethylthiazol-2-yl)-2,5-diphenyltetrazolium bromide) (MTT) assay is presented in Figure SI-9 (Supporting Information). These results are the average of a series of three different experiments. All types of NPs have shown cell viability levels of more than 90% after 72 h, indicating low toxicity of the coated and uncoated chitosan nanocarriers.

Cell viability and IC_{50} results for different types of the synthesized NPs are presented in Figure 3. Figure 3b displays the viability of Caco-2 cells after 72 h exposure to different concentrations of the PTX-loaded NPs as a function of pH at 37 °C. Increasing PTX concentration caused a sharp drop in cell viability.[27] It is also found that pH of the medium plays a leading role in the toxicity of PTX-loaded NPs. Sequential incubation at different pH caused a significant decrease in the Caco-2 cell viability. As stated above, sequential incubations at pH 7.4 and 5.5 lead to dissolution of the outer layer and swelling of inner core, respectively, which resulted in increased release of the drug. There is also a clear relationship between the amount of PTX released and the IC_{50} value. Amoozgar et al. reported incubation of the cells at pH 6.2 with PTX-loaded NPs, coated with a layer of chitosan, caused a significant dose-dependent reduction of the value of cell viability. This trend was comparable to moderate decrease in viability of the cells incubated with the PTX-loaded NPs at pH 7.4.[28] Such pH-dependent cytotoxicity has been reported elsewhere even for neat chitosan-based NPs. Loh et al. reported Caco-2 cellular uptake of chitosan NPs in pH 6.0 results in lower cell viability than at pH 7.4.[29]

Figure 3c illustrates the IC_{50} trend, which shows the effective PTX concentration required for a 50% decrease in cell viability. Results show that for all the PTX-loaded NPs, IC_{50} decreased when applying the pH sequence. This finding implies enhanced efficiency of the PTX-loaded NPs in the sequential incubation at different pH values (4, 7.4, and 5.5). Interestingly, the viability of cells incubated with unloaded NPs varies little with NP properties (flow ratio), again emphasizing the pH dependency of IC_{50} on the drug delivery efficacy of microfluidic NPs synthesized at lower flow ratios.

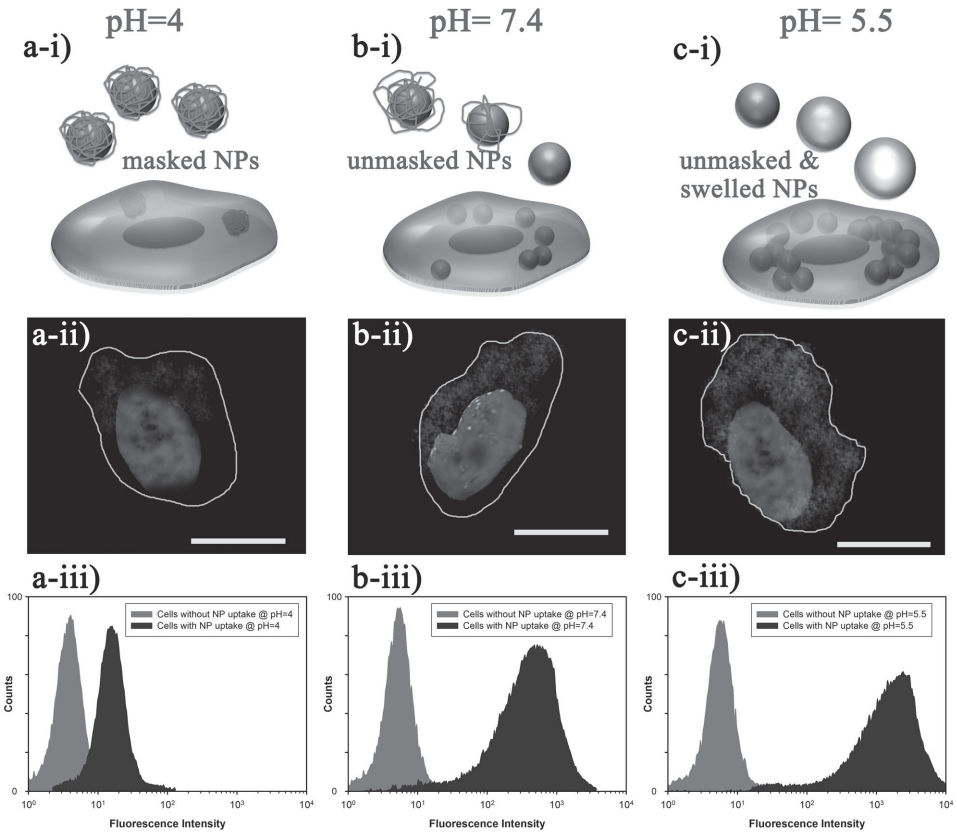

Figure 4. i) Schematic representation of facilitated cellular uptake of NPs after unmasking upon incubation at different pH. ii) Confocal laser scanning microscopy images showing cellular uptake of FITC(Fluorescein isothiocyanate)-labeled HMCS NPs after 2 h incubation with Caco-2 cells after changing the medium pH. Cell nucleus stained with DAPI (4′,6-diamidino-2-phenylindole, blue fluorescence), the green dots represent internalized NPs. Scale bar is 15 μm. iii) Fluorescence-activated cell sorting results of facilitated cellular uptake after unmasking of NPs at different pH.

As shown in **Figure 4**, changing the pH from 4 to 7.4, and then 5.5, results in unmasking of HMCS NPs and facilitated cellular uptake of NPs. It seems masked NPs with anionic surfaces have less interaction with the negatively charged cell membrane, which leads to lower transfection efficiency. It was previously reported that surface charge affects cellular uptake of chitosan-based NPs.[30]

Changing the pH to 7.4 is combined with the dissolution of Eudragit layer and a higher degree of cellular accessibility for unmasked HCMS NPs. Although removing the Eudragit shell generates more cellular transfection, a greater amount of cellular uptake is observed with protonation of amino groups of chitosan as a result of changing the pH from 7.4 to 5.5.[26,31] Due to this charge, as shown in Figure 1c-iv, chitosan NPs are often endocytosed by the cells.[8,32] The cell uptake trend is quantitatively reported in Figure 4iii. The ratio of the florescence intensity for cells with and without NP uptake shows the NPs' uptake efficiency, and increased with altering the pH to 7.4 and then to 5.5. The cellular uptake is positively correlated with the surface charge in the NPs. Normally, transfection efficiency of chitosan is higher for culture medium with a lower pH value due to a higher degree of chitosan protonation.[21,30]

Cellular uptake nanoparticles as a function of applied pH are evaluated in other cancerous cell lines (MCF-7 and HeLa cells) and the results are presented in Figure SI-10 (Supporting Information); the same trends are seen in the other cell lines as well. To investigate the effects of the presence of serum proteins on NPs–cells interactions, cellular uptake of prepared coated and uncoated NPs is measured in serum-based culture (10% Fetal bovine serum (FBS) containing medium) in three different cell lines (Figure SI-10, Supporting Information) as a function of pH and after 2 h of incubation.

Nanoparticle systems, due to their unique features as drug carriers, have attracted a great deal of interest in colon cancer chemotherapy. For the first time, we employed a dual microfluidic procedure to attain highly tunable core–shell drug carriers with customized and reproducible characteristics adjusted for targeted colon cancer therapy. Self-assembled hydrophobically modified chitosan NPs were produced in a cross-junction microfluidic device and finely coated with a pH-sensitive copolymer (Eudragit) through a Tesla micromixer. QM and classical MD simulations indicate a good level of molecular interactions between the layered nanostructures. NPs fabricated and coated via microfluidics showed increased cellular uptake during pH changes compared to those prepared with bulk mixing. MTT assays and in vitro results showed coating the NPs with a pH-sensitive Eudragit layer gives the NPs the ability to bypass the acidic gastric fluid without releasing the majority of the loaded anticancer drug. Considering the pH-sensitive characteristics of the microfluidic NPs, such a highly tunable drug delivery system

enabling physiological-stimuli release is a highly promising route to develop efficient targeting colon chemotherapeutic agents.

Supporting Information

Supporting Information is available from the Wiley Online Library or from the author.

Acknowledgements

M.M.H.-S., S.T., and E.D. contributed equally to this work. The authors would like to thank Dr. H. Van Lintel and M. Taghipoor in the LMIS4-EPFL for their helpful technical assistance and Prof. Jeffrey A. Hubbell (EPFL-IBI-LMRP) for his valuable comments on early stage of this study. This research was performed in the framework of Biologically Inspired Developing Advanced Research (BiDAR) group.

Received: June 6, 2015
Revised: July 20, 2015
Published online: March 22, 2016

[1] A. Kreso, P. Galen, N. M. Pedley, E. L. Fernandes, C. Ferlin, T. Davis, L. Cao, R. Baiazitov, W. Du, N. Sydorenko, Y. C. Moon, L. Gibson, Y. Wang, C. Leung, N. N. Iscove, C. Arrowsmith, C. A. Szentgyorgyi, S. Gallinger, J. E. Dick, J. A. O'Brien, *Nat. Med.* **2014**, *20*, 29.

[2] a) K. A. Paschos, N. Bird, *Hippokratia* **2008**, *12*, 132; b) S. Van Schaeybroeck, W. L. Allen, R. C. Turkington, P. G. Johnston, *Nat. Rev. Clin. Oncol.* **2011**, *8*, 222; c) V. P. Torchilin, *Handbook Exp. Pharmacol.* **2010**, *197*, 3.

[3] a) Z. Cheng, A. Al Zaki, J. Z. Hui, V. R. Muzykantov, A. Tsourkas, *Science* **2012**, *338*, 903; b) B. C. Giovanella, J. S. Stehlin, M. E. Wall, M. C. Wani, A. W. Nicholas, L. F. Liu, R. Silber, M. Potmesil, *Science* **1989**, *246*, 1046; c) V. P. Torchilin, **2010**, *197*, 3; d) M. Loeffler, J. A. Krüger, A. G. Niethammer, R. A. Reisfeld, *J. Clin. Invest.* **2006**, *116*, 1955.

[4] a) D. Shi, N. M. Bedford, H. S. Cho, *Small* **2011**, *7*, 2549; b) M. Ferrari, *Nat. Rev. Cancer* **2005**, *5*, 161; c) K. Thanki, R. P. Gangwal, A. T. Sangamwar, S. Jain, *J. Control. Rel.* **2013**, *170*, 15; d) A. des Rieux, V. Pourcelle, P. D. Cani, J. Marchand-Brynaert, V. Préat, *Adv. Drug Delivery Rev.* **2013**, *65*, 833.

[5] a) K. Y. Win, S. S. Feng, *Biomaterials* **2005**, *26*, 2713; b) R. Khatik, P. Dwivedi, M. Upadhyay, V. K. Patel, S. K. Paliwal, A. K. Dwivedi, *J. Biomater. Tissue Eng.* **2014**, *4*, 143; c) M. V. Srikanth, B. J. Ram, S. A. Sunil, N. S. Rao, K. V. R. Murthy, *Int. J. Pharm. Sci. Rev. Res.* **2011**, *10*, 203.

[6] a) Y. Wang, P. Li, Z. Peng, F. H. She, L. X. Kong, *J. Appl. Polym. Sci.* **2013**, *129*, 714; b) L. F. A. Asghar, M. Azeemuddin, V. Jain, S. Chandran, *Drug Delivery* **2009**, *16*, 205; c) C. A. Schoener, N. A. Peppas, *J. Biomater. Sci. Polym. Ed.* **2013**, *24*, 1027; d) W. Gao, J. M. Chan, O. C. Farokhzad, *Mol. Pharm.* **2010**, *7*, 1913.

[7] C. L. Peng, H. M. Tsai, S. J. Yang, T. Y. Luo, C. F. Lin, W. J. Lin, M. J. Shieh, *Nanotechnology* **2011**, *22*, 265608.

[8] F. S. Majedi, M. M. Hasani-Sadrabadi, J. J. VanDersarl, N. Mokarram, S. Hojjati-Emami, E. Dashtimoghadam, S. Bonakdar, M. A. Shokrgozar, A. Bertsch, P. Renaud, *Adv. Funct. Mater.* **2014**, *24*, 432.

[9] D. Ray, D. K. Mohapatra, R. K. Mohapatra, G. P. Mohanta, P. K. Sahoo, *J. Biomater. Sci. Polym. Ed.* **2008**, *19*, 1487.

[10] M. M. Patel, A. F. Amin, *Drug Delivery* **2011**, *18*, 281.

[11] G. M. Whitesides, *Nature* **2006**, *442*, 368.

[12] F. S. Majedi, M. M. Hasani-Sadrabadi, S. Hojjati Emami, M. A. Shokrgozar, J. J. Vandersarl, E. Dashtimoghadam, A. Bertsch, P. Renaud, *Lab Chip* **2013**, *13*, 204.

[13] S. Taranejoo, M. Janmaleki, M. Rafienia, M. Kamali, M. Mansouri, *Carbohyd. Polym.* **2011**, *83*, 1854.

[14] F. S. Majedi, M. M. Hasani-Sadrabadi, S. Hojjati Emami, M. A. Shokrgozar, J. J. VanDersarl, E. Dashtimoghadam, A. Bertsch, P. Renaud, *Lab Chip* **2013**, *13*, 204.

[15] E. Dashtimoghadam, H. Mirzadeh, F. A. Taromi, B. Nyström, *Polymer* **2013**, *54*, 4972.

[16] M. M. Hasani-Sadrabadi, F. S. Majedi, J. J. Vandersarl, E. Dashtimoghadam, S. R. Ghaffarian, A. Bertsch, H. Moaddel, P. Renaud, *J. Am. Chem. Soc.* **2012**, *134*, 18904.

[17] M. M. Hasani Sadrabadi, V. Karimkhani, F. S. Majedi, J. J. Van Dersarl, E. Dashtimoghadam, F. Afshar-Taromi, H. Mirzadeh, A. Bertsch, K. I. Jacob, P. Renaud, *Adv. Mater.* **2014**, *26*, 3118.

[18] P. Ingram, H. G. Jerrard, *Nature* **1962**, *196*, 57.

[19] J. Fallingborg, *Dan. Med. Bull.* **1999**, *46*, 183.

[20] G. Pye, D. Evans, S. Ledingham, J. Hardcastle, *Gut* **1990**, *31*, 1355.

[21] Z. Du, S. Pan, Q. Yu, Y. Li, Y. Wen, W. Zhang, M. Feng, C. Wu, *Colloids Surf. A: Physicochem. Eng. Asp.* **2010**, *353*, 140.

[22] H. K. Moo, M. H. Su, L. S. Cheon, L. H. Jae, K. Sungwon, P. Kinam, *J. Control. Rel.* **2008**, *126*, 122.

[23] H. M. Ding, Y. Q. Ma, *Sci. Rep.* **2013**, *3*, 2804.

[24] J. Shi, N. M. Alves, J. F. Mano, *Macromol. Biosci.* **2006**, *6*, 358.

[25] A. Popat, J. Liu, G. Q. Lu, S. Z. Qiao, *J. Mater. Chem.* **2012**, *22*, 11173.

[26] W. Chen, J. Du, *Sci. Rep.* **2013**, *3*, 2162.

[27] a) J. E. Liebmann, J. A. Cook, C. Lipschultz, D. Teague, J. Fisher, J. B. Mitchell, *Br. J. Cancer* **1993**, *68*, 1104; b) T. Yang, M. K. Choi, F. D. Cui, S. J. Lee, S. J. Chung, C. K. Shim, D. D. Kim, *Pharm. Res.* **2007**, *24*, 2402.

[28] Z. Amoozgar, J. Park, Q. Lin, Y. Yeo, *Mol. Pharm.* **2012**, *9*, 1262.

[29] J. W. Loh, M. Saunders, L. Y. Lim, *Toxicol. Appl. Pharmacol.* **2012**, *262*, 273.

[30] Z. G. Yue, W. Wei, P. P. Lv, H. Yue, L. Y. Wang, Z. G. Su, G. H. Ma, *Biomacromolecules* **2011**, *12*, 2440.

[31] a) T. Sato, T. Ishii, Y. Okahata, *Biomaterials* **2001**, *22*, 2075; b) B. Sarmento, J. Das Neves, *Chitosan-Based Systems for Biopharmaceuticals: Delivery, Targeting and Polymer Therapeutics*, John Wiley & Sons, Hoboken, NJ, USA, **2012**.

[32] T.-G. Iversen, T. Skotland, K. Sandvig, *Nano Today* **2011**, *6*, 176.